ACS NANO
Cite This: ACS Nano 2019, 13, 6083−6089
www.acsnano.org

ARTICLE

Single-Layered MoS_2 Directly Grown on Rutile TiO_2(110) for Enhanced Interfacial Charge Transfer

Huihui Liu,[†,#] Yue Li,[‡,#] Miaomiao Xiang,[†] Hualing Zeng,[*,‡,§,∥] and Xiang Shao[*,†,∥,⊥]

[†]Department of Chemical Physics, [‡]International Center for Quantum Design of Functional Materials (ICQD), Hefei National Laboratory for Physical Sciences at the Microscale, [§]Key Laboratory of Strongly-Coupled Quantum Matter Physics, Chinese Academy of Sciences, Department of Physics, [∥]Synergetic Innovation Center of Quantum Information and Quantum Physics, and [⊥]CAS Key Laboratory of Urban Pollutant Conversion, University of Science and Technology of China, Hefei, Anhui 230026, China

Supporting Information

ABSTRACT: **Interfacial charge transfer is critical for the photocatalytic activities of compositional photocatalysts. In this work, we have developed a strategy of growing single-layer MoS_2 sheets on the rutile TiO_2(110) single-crystal surface using a chemical vapor deposition method. Both on-site and off-site characterizations confirmed the monolayer thickness and single crystallinity of the MoS_2 adlayer as well as the atomic flatness of the composite surface. Without the presence of contamination, the charge flow across the interface of MoS_2 and TiO_2 is greatly enhanced, which hence favors the charge separation under excitations and boots up the catalytic activity of the composite system. Moreover, we found the luminescing property of MoS_2 is significantly tailored upon coupling with the TiO_2 surface. Our work has established a method for revealing the interface properties of the transition-metal dichalcogenides and oxide semiconductors at the atomic level.**

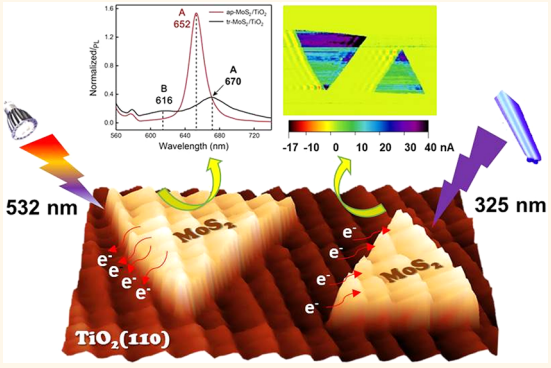

KEYWORDS: *MoS_2, rutile-TiO_2, interface, CVD, charge transfer*

As a prototypical heterostructure of transition-metal dichalcogenides (TMDs) and oxide semiconductors, the MoS_2/TiO_2 composite has received increasing research interests due to its potential applications in electronics,[1,2] photovoltaics,[3] and in particular, photocatalysis.[4,5] Theoretically, the TMDs are characteristic of sufficiently high electron conductivity and mobility[6] while the oxides, TiO_2 and ZnO for instance, possess relatively large band gap yet meantime the proper anchoring sites for molecular reactions.[7,8] Their combination constitutes heterojunction wherein the intrinsic properties of the two materials are fairly preserved except at the interface region an dipole field is established.[9−11] The latter can take an active effect in separating the photoinduced carriers, which thus leads to increased visible light absorption and enhanced redox reactivities.[12,13]

Experimentally, the heterojunction of TMDs and oxides was usually prepared *via* hydrothermal synthesis or other wet chemical methods.[14,15] It is the applied solution environments that inevitably cause large amounts of adsorbates to be intercalated in the TMD/oxide interface or strongly bound on the surface, which can severely weaken the hybridization and, hence, hamper the charge transfer between TMD and oxide. As a solution, vacuum preparation[16] or chemical vapor deposition (CVD) strategies[17−19] can perfectly avoid such problems because of their clean/inert atmosphere and high synthetic temperatures. Recently, there has much progress in preparing MoS_2 or analogue TMDs on various oxide surfaces *via* the CVD method.[20−25] However, direct synthesis of MoS_2 on a reducible oxide surface such as TiO_2 remains a challenge considering the ease of reduction and corrosion of the TiO_2 surface.[9,10,25] In this work, we report that high-quality MoS_2 sheets can be grown on a rutile TiO_2(110) single-crystal surface by using MoO_3 and sulfur as the reagents of a CVD process. Rutile TiO_2(110) was chosen as the substrate because of its fairly good thermal stability, well-understood surface structure, and the easy availability of single crystals, all perfectly fitting the criteria for constructing a model system. With the optimized synthetic parameters in hand, the atomic flatness of the TiO_2(110) surface was well preserved, while the MoS_2 was fabricated with single crystallinity and monolayer thickness and

Received: April 4, 2019
Accepted: May 2, 2019
Published: May 2, 2019

DOI: 10.1021/acsnano.9b02608
ACS Nano 2019, 13, 6083−6089

intimately attached to the substrate. Moreover, subsequent characterizations clearly reveal that without the presence of intercalated species the interfacial charge transfer between MoS_2 and TiO_2 is substantially enhanced under various illuminating conditions, and the luminescing property of MoS_2 is significantly tailored. This work has deepened our understandings of the TMDs/oxide heterojunctions at an atomic level.

RESULTS AND DISCUSSION

Characterization of the As-Prepared MoS_2 Sheets on TiO_2(110). Figure 1 shows a series of characterizations of the as-prepared MoS_2 on TiO_2 substrate (termed as ap-MoS_2/TiO_2). The atomic force microscopy (AFM) image in Figure 1a clearly shows the triangular-shaped MoS_2 sheets randomly dispersed on the r-TiO_2(110) substrate whose atomic flatness and the step-terrace structure are well preserved. The MoS_2 sheets are measured as wide as 1−3 μm and as thick as ∼0.7 nm, consistent with the height of a single-layer MoS_2. Topographically, the synthesized MoS_2 is found closely attached to the TiO_2 surface, even at the step region. To characterize *in situ* the atomic structure of the synthesized MoS_2 nanosheet, we have performed the same CVD growth on a Nb-dope TiO_2(110) singlecrystal substrate (shortened as Nb:TiO_2(110)) and obtained identical AFM topographies as on undoped TiO_2 substrate, as shown in Figure S1. Figure 1b and the inset show the large-area and atomically resolved scanning tunneling microscope (STM) images of the as-prepared MoS_2/Nb:TiO_2(110) sample, respectively, which unambiguously confirm the atomic structure of MoS_2. One may notice the corrugated pattern resolved on the MoS_2 patch. We tentatively attribute it to single-layer vacancies distributed at the TiO_2 substrate underneath the MoS_2 sheet since they have the same depth as a single step on TiO_2(110). Moreover, Figure S2a,b clearly shows the continuous MoS_2 lattice crossing both the step and the vacancy features of the TiO_2 substrate, demonstrating the single crystallinity of the MoS_2 sheet. Besides the AFM/STM measurements, the ultraviolet−visible absorption spectroscopy (UV−vis) of the ap-MoS_2/TiO_2 sample shows slightly enhanced absorbance of visible light relative to the blank TiO_2, as presented in Figure 1c. The inset shows the intentionally magnified visible light region wherein the characteristic absorptions of MoS_2 at around 650 and 605 nm can be clearly identified.[20] Figures 1d−f show the scanning electron microscopy (SEM) image as well as the corresponding elemental mapping of Mo (Figure 1e) and S (Figure 1f), which also strongly support the formation of MoS_2 on TiO_2 surface.

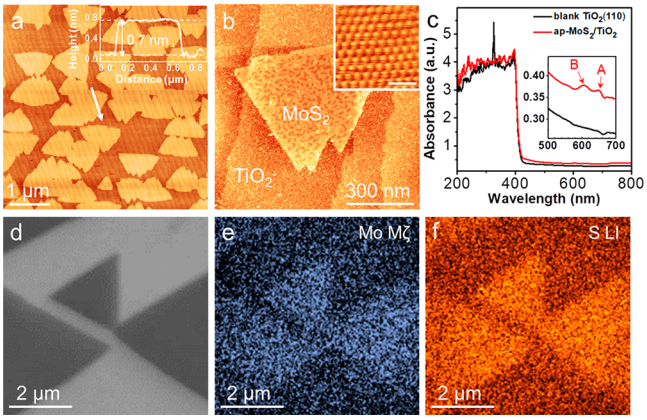

Figure 1. Characterizations of the as-grown MoS_2 sheets on an r-TiO_2(110) single-crystal substrate. (a) AFM topographic image of the ap-MoS_2/TiO_2(110) sample surface. The inset shows the height profile of a MoS_2 sheet. (b) STM image of a specially small MoS_2 nanosheet grown on an Nb-doped r-TiO_2(110) surface. The inset shows the atomic resolution. The scale bar is 1 nm. (c) UV−vis spectra of the blank TiO_2 (black) and the ap-MoS_2/TiO_2 (red). Inset is the magnified spectrum of the visible-light regime where the characteristic absorption of MoS_2 can be identified. (d−f) SEM image and elemental mapping (e for Mo and f for S) of a selected region on the ap-MoS_2/TiO_2 sample. The triangular dark features in (d) correspond to MoS_2.

For better evaluating the quality of the synthesized MoS_2, we performed procedures to peel it off the TiO_2 substrate by following the reported recipe on similar TMD/oxide systems.[9,26,27] Figure 2a shows the SEM images of the MoS_2 transferred onto a SiO_2/Si surface, which clearly attests that the transfer operation is successful but some of the MoS_2 sheets (marked by the white arrows) are unavoidably broken during the transfer. Figure 2b shows the Raman spectrum taken on the transferred MoS_2/SiO_2/Si. The two characteristic peaks, 384 and 404 cm^{-1}, can be clearly identified and are ascribed to the E^1_{2g} and A_{1g} phonon modes of MoS_2, respectively.[20,28] Noticeably, the interval between E^1_{2g} and A_{1g} peaks (≤20 cm^{-1}) strongly supports that our MoS_2 is perfectly single layer. We also directly measured Raman spectroscopy on the ap-MoS_2/TiO_2 samples, but the MoS_2 signals are completely buried by the strong background signal of TiO_2, as shown in Figure S3. Parts c and d of Figure 2 show the AFM topography and corresponding phase images of the transferred MoS_2 sheets on the SiO_2/Si substrate. From the profile, one immediately notices that the SiO_2/Si substrate possesses a much rougher surface than TiO_2(110), and the transferred MoS_2 shows a thickness larger than 1.0 nm,

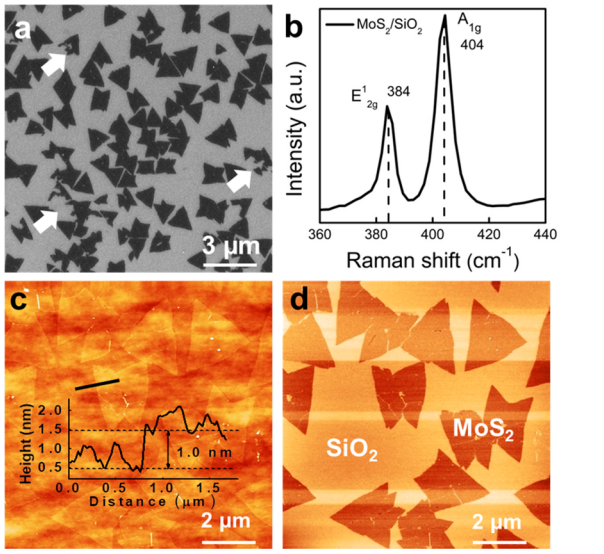

Figure 2. (a) SEM image and (b) Raman spectrum of the MoS_2 transferred onto a SiO_2/Si substrate. White arrows mark the broken MoS_2 sheets due to the transfer operation. (c, d) AFM topography and the corresponding phase images of the MoS_2/SiO_2/Si surface sample. (c, inset) Height profile along the black line which runs across the edge of a MoS_2 sheet.

DOI: 10.1021/acsnano.9b02608
ACS Nano 2019, 13, 6083−6089

significantly higher than that of ap-MoS_2/TiO_2, which is possibly due to the presence of the intercalated species.

The peeled MoS_2 also renders the direct characterization with transmission electron microscopy (TEM). Parts a and b of Figure 3 show the large area and atomically resolved image

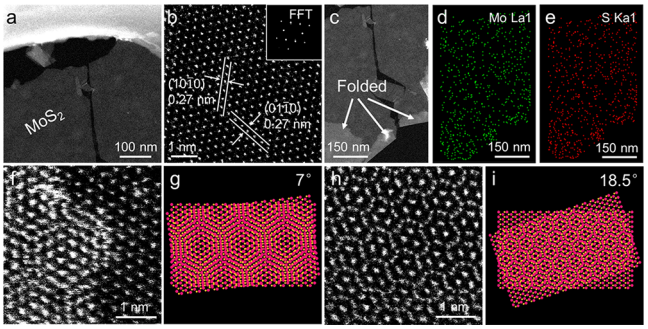

Figure 3. TEM characterization of the MoS_2 transferred to a copper mesh. (a, b) Typical low- and high-resolution TEM images of the prepared MoS_2. (b, inset) is the FFT image showing the periodicity of the MoS_2 lattice. (c) Selected low-magnification image and corresponding (d) Mo and (e) S mapping of a MoS_2 film containing folded regions which is formed during the transfer process. (f, h) High-resolution images of different folded areas with distinct moiré patterns; corresponding models are given in (g) and (h), respectively.

of the MoS_2 transferred onto a copper mesh. Both the interplane spacing measurement and the fast Fourier transformation (FFT) result in a lattice constant of 0.27 nm, which perfectly coincides with the reported value of MoS_2(0001).[20,29] Figure 3c shows a selected edge area of MoS_2, where film backfolding and overlaying can be observed. The elemental mapping of both Mo and S (parts d and e, respectively, of Figure 3) perfectly reproduces the observed shape of the MoS_2 sheet, once again proving the composition. For the folded region, high-resolution images (Figures 3f,h) show different moiré patterns, which can be modeled by rotational stacking of two MoS_2 layers with angles of 7° (Figure 3g) and 18.5° (Figure 3i), respectively.

XPS Measurements of the Various MoS_2/TiO_2 Samples. Once the single-layer thickness and single crystallinity of the fabricated MoS_2 have been confirmed, we can examine the status of the MoS_2/TiO_2 interface. Figure 4 shows the X-ray photoelectron spectroscopy (XPS) spectra taken on a typical ap-MoS_2/TiO_2 sample. The full-range survey spectrum is presented in Figure S4, from which the cleanness of the compositional system can be evidenced. The high-resolution Mo 3d spectrum in Figure 4a demonstrates the dominance of Mo^{4+}, whose $3d_{5/2}$ and $3d_{3/2}$ were found at 229.8 and 233.0 eV, respectively, consistent with that reported for MoS_2 in the literature.[30] At the same time, trace amounts of Mo^{5+} and Mo^{6+} were also observed, possibly due to the unreacted MoO_3 particles (Figure S5) or air-induced oxidation of MoS_2 at the defect sites. On the lower binding energy (BE) side of Mo 3d a prominent S 2s transition is also clearly recognized, demonstrating the S component of MoS_2. After MoS_2 was peeled off, no detectable Mo and S signals were found on the stripped TiO_2(110) (termed as st-TiO_2(110)) sample, as shown in Figure S6.

In Figure 4b,c we show the sequence of XPS spectra of Ti 2p and O 1s obtained on four different samples, *i.e.*, the blank TiO_2(110), the ap-MoS_2/TiO_2, the st-TiO_2(110), and the MoS_2/TiO_2 composite obtained by transferring MoS_2 back onto a bare r-TiO_2(110) surface (termed as tr-MoS_2/TiO_2). It can be clearly seen that in the presence of MoS_2 both Ti 2p and O 1s are shifted to higher BE synchronically by 0.5−0.6 eV, while those of blank TiO_2(110) and st-TiO_2(110) are essentially the same. In Figure S7a,b we show the deconvolution of the Ti 2p and O 1s spectra of ap-MoS_2/TiO_2, respectively. No identifiable signatures for the Ti^{3+} species can be observed, although they were frequently observed in the composite of TiO_2 and MoS_2 fabricated by other methods. In Figure S7c,d we arbitrarily shift each Ti 2p (O 1s) spectrum to the same binding energy and normalize them to the same intensity, in order to check the profile changes. Noticeably, all four samples show the exact overlapping of the Ti 2p spectra, manifesting the absence of Ti^{3+} formation during the CVD growth. In contrast, the O 1s of tr-MoS_2/TiO_2 shows significantly increased OH features, dictating the introduced intercalation during the wet treatments. With these detailed analyses, the blue-shifts in the BE of both Ti 2p and O 1s of the ap-MoS_2/TiO_2 samples can be attributed to the static field established at the interface, similar to the cases of graphene grown on TiO_2 and ZnO surfaces.[9]

The static electric field at the MoS_2/TiO_2 interface should originate from the work function difference between MoS_2 and TiO_2. A direct proof of such proposition comes from the Kelvin probe force microscopy (KPFM) measurements of the MoS_2/TiO_2 sample. As shown in Figure 5, the surface potential image clearly evidences a lower contact potential (∼−0.1 V) in the MoS_2 region and a higher contact potential (∼0.1 V) in the uncovered TiO_2 region of the ap-MoS_2/TiO_2 sample surface, as compared with the AFM tip. This means in

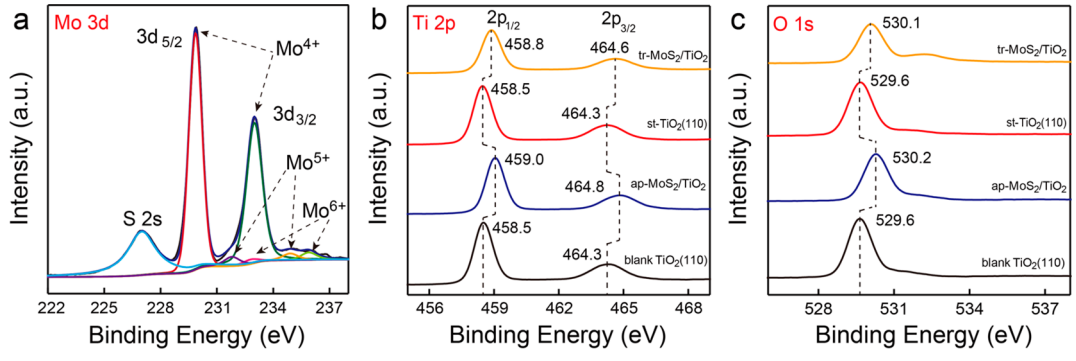

Figure 4. (a) High-resolution XPS spectrum of Mo 3d on the ap-MoS_2/TiO_2 sample surface. (b, c)Series XPS spectra of Ti 2p and O 1s collected on different surfaces of blank TiO_2(110), ap-MoS_2/TiO_2, st-TiO_2(110), and tr-MoS_2/TiO_2, respectively.

DOI: 10.1021/acsnano.9b02608
ACS Nano 2019, 13, 6083−6089

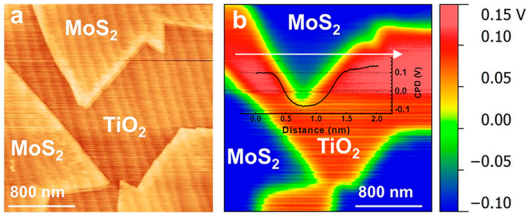

Figure 5. (a) Topography and (b) corresponding surface potential image of an ap-MoS_2/TiO_2 sample measured by KPFM. (b, inset) Line profile along the white arrow, indicating that the MoS_2 region has ∼−0.1 V while the TiO_2 region has ∼0.1 V surface potential relative to the AFM tip.

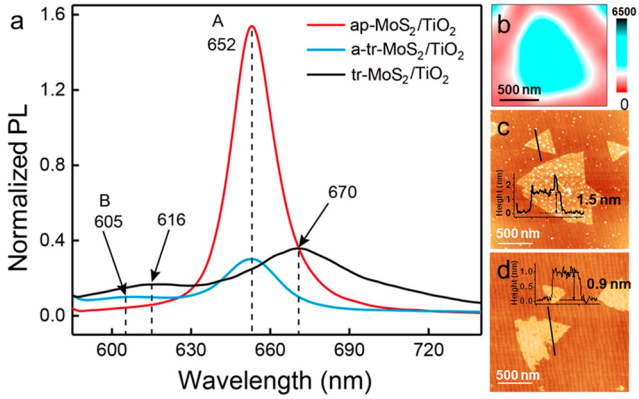

Figure 6. (a) Photoluminescence spectra of ap-MoS_2/TiO_2 (red) and tr-MoS_2/TiO_2 samples with (blue) and without (black) annealing treatment. With intercalated species present, the A and B peaks of the tr-MoS_2/TiO_2 samples were observed to shift to lower energy. (b) Photoluminescence mapping taken with 652 nm wavelength on a MoS_2 sheet of the ap-MoS_2/TiO_2 sample. (c, d) AFM images of a typical tr-MoS_2/TiO_2(110) sample before (c) and after (d) thermal annealing at 400 °C in nitrogen atmosphere. (c, d, insets) Profiles across individual MoS_2 sheets demonstrating that the annealing treatment is able to remove most of the surface adsorbates and the intercalated species but can also lead to the corruption of MoS_2.

the MoS_2-covered region the MoS_2 adlayer donates electrons to the TiO_2 substrate across the interface due to the work function difference. The redistributed charges around the MoS_2/TiO_2 interface thus construct a dipole field pointing along the surface normal. In this regard, introduction of any intercalation species may lead to a reduced interface dipole and, hence, a smaller shift of BE relative to the ap-MoS_2/TiO_2 sample, which has a clean interface, as has been demonstrated by the series of XPS spectra in Figure 4. To support the above idea, we also conducted control experiments by measuring the KPFM of both ap-MoS_2/TiO_2 and the tr-MoS_2/SiO_2 samples with a different AFM tip. As shown in Figure S8, due to the blocked charge transfer the MoS_2 nanosheets on SiO_2 have obviously higher surface potential than on the TiO_2 substrate and show little difference (∼-20 mV) against the SiO_2 surface. In contrast, the ap-MoS_2/TiO_2 sample still shows clear surface potential difference in MoS_2 and TiO_2 regions, respectively, in line with the proposed charge transfer between the two materials.

Photoluminescence Property of the MoS_2/TiO_2 Samples. For MoS_2, due to its semiconducting nature, the optical property is attractive and important. It can be significantly affected by the substrate, the surface, as well as the interface. In Figure 6a, we present the photoluminescence (PL) spectra collected on various different MoS_2/TiO_2 samples. As can be seen, the PL spectrum of the tr-MoS_2/TiO_2 sample shows two peaks centered at 670 and 616 nm upon excitation of the 532 nm laser. They correspond to the A and B excitonic optical transitions in the K/K' valleys of monolayer MoS_2, which originate from the spin−orbit coupling induced band splitting.[31,32] In contrast, the spectrum of the ap-MoS_2/TiO_2 sample shows a single peak which is highly symmetric and centered at 652 nm. This peak should also correspond to the A excitonic emission of MoS_2 yet with slight blue shift in energy (∼51 meV) if compared with tr-MoS_2/TiO_2 and the results from previous reports. A PL mapping of the ap-MoS_2/TiO_2 taken at this peaking wavelength is shown in Figure 6b, demonstrating the luminescing uniformity of the fabricated MoS_2 nanosheet. It is well-known that the MoS_2 emission can be affected by the dielectric surroundings.[33,34] However, the built-in screening effect of TiO_2 substrate merely cannot explain the observed blue shift in the emission of the ap-MoS_2/TiO_2. Other contributions have to be taken into account, which leads us to the dipole field established at the MoS_2/TiO_2 interface. Considering that the electron affinity of monolayer MoS_2 (4.5 eV)[35] is lower than that of TiO_2 (5.2 eV),[36,37] the perfect coupling at the interface of the ap-MoS_2/TiO_2 sample will generate a perpendicular electric field at the interface, resulting in band renormalization in MoS_2. It has been predicted that applying an electric field perpendicular to the 2D plane can modify the on-site energy of atoms in MoS_2, which tailors its electronic structure.[38] Under the positive perpendicular electric field, the bandgap at K/K' valleys will be enlarged, resulting in the blue shift of the PL peaks. As a control experiment, we show that the perfect coupling at the MoS_2/TiO_2 interface can be re-established by annealing after the peeling off and transfer processes. By additionally annealing the tr-MoS_2/TiO_2 sample (hence termed as a-tr-MoS_2/TiO_2), we found that the PL spectrum gradually approached the ap-MoS_2/TiO_2 case, showing the A peak at ∼652 nm and concomitantly an observable B peak at ∼605 nm. Correspondingly, the AFM measurements shown in Figures 6c,d clearly confirm that the postannealing treatment can efficiently remove most of the surface adsorbates and the intercalated species (see the comparison of the profiles), thus re-establishing the interface between MoS_2 and TiO_2. It also significantly degrades the MoS_2 sheets by creating a considerable number of defects. With the above statements, the blueshift of the A excitonic emission relative to the intrinsic MoS_2 confirms the existence of the dipole field in the ap-MoS_2/TiO_2 interface. We also measured the PL of the ap-MoS_2/TiO_2 under the excitation of UV light with 325 nm wavelength as shown in Figure S9. The spectrum shows a single peak at around 660 nm yet with much lower intensity. In this case, the TiO_2 substrate can be excited. The photoinduced electrons in the TiO_2 substrate may donate back into MoS_2, which hence reduces the dipole field at the interface. As a consequence, the PL peak from MoS_2 greatly weakens and redshifts slightly.

Photocurrent Responses of the MoS_2/TiO_2 Composite. Finally, the most expected consequence of a clean MoS_2/TiO_2 heterojunction is the improved photoactivity of the composite. With our model system, we can directly investigate the interfacial charge-transfer behavior upon light irradiation at the absence of interface contaminations. Parts a and b of

DOI: 10.1021/acsnano.9b02608
ACS Nano 2019, 13, 6083−6089

Figures 7 show the tunneling AFM (TUNA) measurements of an ap-MoS_2/TiO_2 sample prepared on a 0.5%Nb-doped

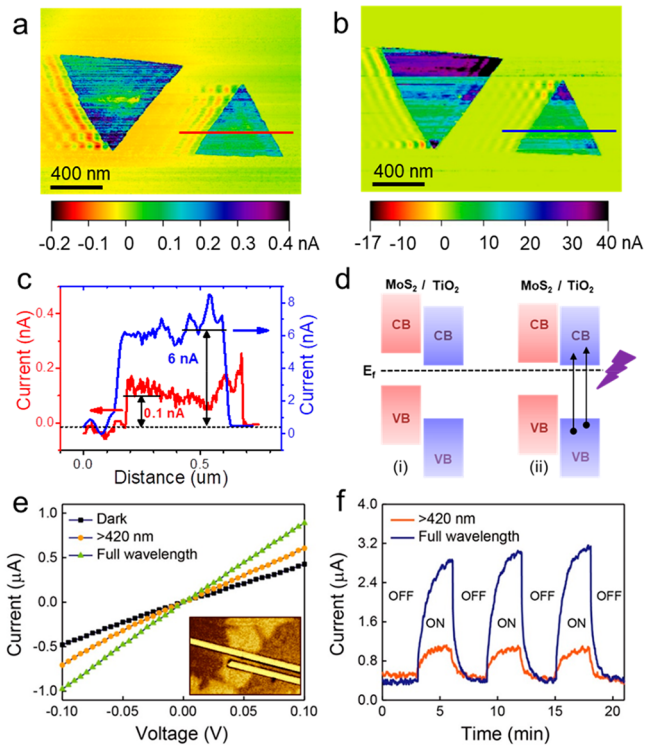

Figure 7. Tunneling AFM measurements of the MoS_2 sheet prepared on a 0.5% Nb-doped TiO_2(110) substrate under (a) dark conditions and (b) continuous irradiation of UV light. (c) Current profiles along the red and blue lines in (a) and (b), respectively. (d) Schematic model shows the electron excitation in TiO_2 upon UV light irradiation and the subsequent band realignment at the interface. CB and VB denote conduction and valence bands, respectively. (e) Current−voltage curves measured with two electrodes directly deposited on a MoS_2 sheet. (Inset) SEM image of the setup. (f) Current responses to the switching on/off of the visible (orange) and full-range (blue) light irradiations. The bias was fixed at 100 mV.

TiO_2(110) substrate under dark and UV light illumination conditions, respectively. From the profiles shown in Figure 7c one can clearly see that even under dark conditions the MoS_2-covered area already shows increased out-of-plane conductivity compared to the bare Nb:TiO_2 surface. Upon switching on the UV light with a power of 5 W and centered wavelength of 365 nm, the conductivity of the MoS_2 area is dramatically enhanced by almost 2 orders of magnitude, while the uncovered TiO_2 remains more or less the same as in darkness. In a control experiment shown in Figure S10, another MoS_2 sheet is imaged with and without a normal illuminating torch (visible light) switched on, which shows an ignorable difference. Therefore, the observed significant increase of the tunneling current under UV light can be ascribed to the sufficient charge transfer from TiO_2 into MoS_2 since TiO_2 is a bulk material and can be readily excited under UV irradiations. In this case, the energy difference between the conduction bands of MoS_2 and TiO_2 may be reduced, which thus facilitates the charge transfer from TiO_2 to MoS_2, as presented by the schematic model in Figure 7d. Better understanding of the MoS_2/TiO_2 heterojunction can be obtained from the in-plane conductivity changes under different irradiation conditions. As shown in Figure 7e and the inset, two gold electrodes with interval of 1 μm were deposited onto a single MoS_2 sheet, and the current responses were collected during ramping of the bias. In this case, the irradiations were provided by a xenon lamp with power of 150 W. The conductance of the MoS_2/TiO_2 composite was measured to be 4.4, 6.4, and 9.3 $S{\cdot}m^{-1}$ for dark, visible-light, and full-length irradiations, respectively. Figure 7f shows the current signal changes upon switching the light on/off repeatedly, which also presents an on/off response except for the relatively slow response speed. The related charge-transfer dynamics will be investigated with time-resolved photoelectron spectroscopy and reported in a separated work. Nevertheless, the above measurements clearly demonstrate that the photoexcited electrons in TiO_2 are efficiently transferred into MoS_2 without interruption of the intercalated species. Consequently, the separated photoelectrons and holes, respectively, render the reduction and oxidation reactions at the corresponding surface sites.

CONCLUSION

In conclusion, by using MoO_3 and sulfur powder as solid precursors for CVD growth, we have successfully synthesized high-quality single-layer MoS_2 sheets on the atomically flat r-TiO_2(110) single-crystal surface. Detailed characterizations including AFM/STM, XPS, and PL measurements not only confirmed the seamless contact between MoS_2 and TiO_2 but also unambiguously revealed the efficient electron transfer across the intimate MoS_2/TiO_2 heterojunction under different irradiation conditions. Our work has provided a strategy of establishing proper TMD/oxide model systems for a deepened understanding of the corresponding photocatalytic mechanisms.

MATERIALS AND METHODS

Materials. (1) Rutile TiO_2(110) (r-TiO_2(110), 10 × 5 × 0.5 mm^3, 99.99%, Hefei Kejing Material Technology Co., Ltd.). (2) 0.5% Nb-doped r-TiO_2(110) (10 × 3 × 0.5 mm^3, Shinkosha Co., Ltd.). (3) Silica substrate (SiO_2/Si, Hefei Kejing Material Technology Co., Ltd.). (4) MoO_3 (Aladdin, 99.6%). (5) Sulfur powder (Aladdin, 99.6%), (6) N_2 (Linde industrial gas, 99.999%). (7) Hydrofluoric acid (HF, Sinopharm Chemical Reagent Co., Ltd.). (8) Acetone (Sinopharm Chemical Reagent Co., Ltd., 99.5%). (9) Deionized water (Millipore, Conductivity 18.2 MΩ·cm). All of the chemicals mentioned above were used as received.

Preparation of the Atomically Smooth r-TiO_2 (110) Surface. Atomically smooth surfaces of r-TiO_2(110) were routinely achieved by following a procedure reported by Yamamoto *et al.*,[39] which proceeds sequentially through ultrasonic cleaning with acetone and ultrapure water, etching with 20% HF for 10 min, rinsing with water, drying in a nitrogen stream, and annealing at 800 °C for 3 h in air. The atomic flatness and cleanness of the prepared surfaces were confirmed by AFM and XPS measurements repeatedly. All chemical reagents were directly used without further purification.

CVD Growth of MoS_2. The CVD growth of MoS_2 on the clean r-TiO_2(110) single crystal was performed in a tube furnace (OTF-1200X, Hefei Kejing Material Technology Co., Ltd.) with a dual temperature zone. The specific steps are as follows: (1) Place 120 mg of sulfur powder and 6 mg of MoO_3 in a separated quartz boat and place them, respectively, at the low temperature (set to 200 °C) and high temperature zone (set to 700 °C) of the tube furnace. (2) Put the r-TiO_2(110) substrate upside down in the same quartz boat approximately 2 cm before the MoO_3 powder. (3) Flush the furnace tube with N_2 gas (flow rate ~300 ccm) for 20 min to completely remove the residual oxygen air. (4) Heat the MoO_3 zone to 100 °C under N_2 flow for 1 h to remove the adsorbed water. (4) Reduce the flow rate of N_2 to 10 sccm and heat the MoO_3 zone with a heating

DOI: 10.1021/acsnano.9b02608
ACS Nano 2019, 13, 6083−6089

rate of 15 °C/min. (5) When the MoO_3 zone reaches ~380 °C, the temperature of the sulfur zone begins to rise slowly. Finally the MoO_3 zone reaches 700 °C, and the sulfur zone reaches 200 °C. (6) Keep both zones at the target temperature for 10 min before turning off the heating. (7) Let the furnace cool down naturally until it reaches approximately 580 °C. Afterward, increase the N_2 flow rate to 300 ccm and open the shroud of the furnace to speed the cooling to room temperature. With this procedure, single-layered MoS_2 with a crystal size of 1−5 μm can be prepared.

Characterization Methods. All atomic force microscopy measurements were performed on a Multimode AFM V produced by Bruker under ambient conditions. The images were obtained with commercial silicon cantilevers from the same company. In particular, topographic images were measured with a standard silicon cantilever. Kelvin probe force microscopy (KPFM) was measured with As-doped silicon tips with different coatings (SCM-PIT-V2 or MESP, Bruker Co.). Tunneling AFM (TUNA) was measured with an As-doped silicon tip with resistivity of 0.01−0.025 Ohm·cm (SCM-PIC, Veeco Co.). For TUNA measurements under illumination conditions, electric torches with similar power (~5 W) but different center wavelengths were applied to mimic the visible-light and UV-light irradiations, respectively.

Scanning tunneling microscopy (STM) was measured with a commercial low-temperature STM (Createc) operated at liquid nitrogen temperature. The samples were slightly degassed to around 100 °C in the fast-entry chamber with pressure of 1×10^{-7} mbar before being transferred into STM. The UV−vis absorption spectra were acquired on a SolidSpec-3700 spectrometer (Shimazu). TEM images were obtained by ARM-200F (JEOL). SEM measurements were performed using a SIRION 200 (FEI) model instrument. The XPS was measured with an AXIS Ultra (Kratos Analytical) instrument equipped with an Al Kα source (1486.7 eV). PL measurements were conducted using an Iso Plan SCT 320 (Princeton) spectrometer. An excitation laser of 532 nm for the wavelength and 1.5 mW for the power was applied. The laser spot has a diameter as small as 1 μm. Raman spectroscopy was measured using a LabRamHR Raman spectrometer with an excitation light of 514.5 nm.

ASSOCIATED CONTENT

Supporting Information

The Supporting Information is available free of charge on the ACS Publications website at DOI: 10.1021/acsnano.9b02608.

Additional characterization results of the MoS_2/TiO_2 samples including AFM, XPS, PL, and TUNA measurements (PDF)

AUTHOR INFORMATION

Corresponding Authors

*E-mail: hlzeng@ustc.edu.cn. Tel: +86-551-63600062.
*E-mail: shaox@ustc.edu.cn. Tel: +86-551-63600765.

ORCID

Hualing Zeng: 0000-0001-5869-9553
Xiang Shao: 0000-0002-8768-4366

Author Contributions

#H.L. and Y.L. contributed equally to this work.

Notes

The authors declare no competing financial interest.

ACKNOWLEDGMENTS

We are grateful for financial support from the National Key Research and Development Program of China (Grant Nos. 2017YFA0205003, 2017YFA0205004, 2018YFA0306600), NSFC (91545128, 21333001, 11674295), the Fundamental Research Funds for the Central Universities (Grant No. WK2340000082), Anhui Initiative in Quantum Information Technologies (Grant No. AHY170000), and the Thousand Talent Program for Young Outstanding Scientists of the Chinese government.

REFERENCES

(1) Zeng, H.; Dai, J.; Yao, W.; Xiao, D.; Cui, X. Valley Polarization in MoS_2 Monolayers by Optical Pumping. *Nat. Nanotechnol.* **2012**, *7*, 490−493.

(2) Radisavljevic, B.; Radenovic, A.; Brivio, J.; Giacometti, V.; Kis, A. Single-Layer MoS_2 Transistors. *Nat. Nanotechnol.* **2011**, *6*, 147−150.

(3) Liang, J.; Li, J.; Zhu, H.; Han, Y.; Wang, Y.; Wang, C.; Jin, Z.; Zhang, G.; Liu, J. One-Step Fabrication of Large-Area Ultrathin MoS_2 Nanofilms with High Catalytic Activity for Photovoltaic Devices. *Nanoscale* **2016**, *8*, 16017.

(4) Xiang, Q.; Yu, J.; Jaroniec, M. Synergetic Effect of MoS_2 and Graphene as Cocatalysts for Enhanced Photocatalytic H_2 Production Activity of TiO_2 Nanoparticles. *J. Am. Chem. Soc.* **2012**, *134*, 6575−6578.

(5) Yuan, Y. J.; Ye, Z. J.; Lu, H. W.; Hu, B.; Li, Y. H.; Chen, D. Q.; Zhong, J. S.; Yu, Z. T.; Zou, Z. G. Constructing Anatase TiO_2 Nanosheets with Exposed (001) Facets/layered MoS_2 Two-Dimensional Nanojunctions for Enhanced Solar Hydrogen Generation. *ACS Catal.* **2016**, *6*, 532−541.

(6) Niu, M.; Cheng, D.; Cao, D. Understanding the Mechanism of Photocatalysis Enhancements in the Graphene-Like Semiconductor Sheet/TiO_2 Composites. *J. Phys. Chem. C* **2014**, *118*, 5954−5960.

(7) Bai, S.; Wang, L.; Chen, X.; Du, J.; Xiong, Y. Chemically Exfoliated Metallic MoS_2 Nanosheets: A Promising Supporting Co-Catalyst for Enhancing the Photocatalytic Performance of TiO_2 Nanocrystals. *Nano Res.* **2015**, *8*, 175−183.

(8) Zhang, J.; Zhang, L.; Yu, W.; Jiang, F.; Zhang, E.; Wang, H.; Kong, Z.; Xi, J.; Ji, Z. Novel Dual Heterojunction between MoS_2 and Anatase TiO_2 with Coexposed {101} and {001} Facets. *J. Am. Ceram. Soc.* **2017**, *100*, 5274−5285.

(9) Liu, H.; Zhu, D.; Shi, H.; Shao, X. Fabrication of a Contamination-Free Interface between Graphene and TiO_2 Single Crystals. *ACS Omega* **2016**, *1*, 168−176.

(10) Liu, H.; Chen, Z.; Zhang, L.; Zhu, D.; Zhang, Q.; Luo, Y.; Shao, X. Graphene Grown on Anatase−TiO_2 Nanosheets: Enhanced Photocatalytic Activity on Basis of a Well-Controlled Interface. *J. Phys. Chem. C* **2018**, *122*, 6388−6396.

(11) Liu, H.; Xiang, M.; Shao, X. Graphene/ZnO Nanocomposite with Seamless Interface Renders Photoluminescence Quenching and Photocatalytic Activity Enhancement. *J. Mater. Sci.* **2018**, *53*, 13924−13935.

(12) Long, R.; English, N. J.; Prezhdo, O. V. Photo-Induced Charge Separation across the Graphene-TiO_2 Interface is Faster than Energy Losses: a Time-Domain *Ab Initio* Analysis. *J. Am. Chem. Soc.* **2012**, *134*, 14238−14248.

(13) Long, R.; Casanova, D.; Fang, W. H.; Prezhdo, O. V. Donor-Acceptor Interaction Determines the Mechanism of Photoinduced Electron Injection from Graphene Quantum Dots into TiO_2: π-Stacking Supersedes Covalent Bonding. *J. Am. Chem. Soc.* **2017**, *139*, 2619−2629.

(14) Cravanzola, S.; Muscuso, L.; Cesano, F.; Agostini, G.; Damin, A.; Scarano, D.; Zecchina, A. MoS_2 Nanoparticles Decorating Titanate-Nanotube Surfaces: Combined Microscopy, Spectroscopy, and Catalytic Studies. *Langmuir* **2015**, *31*, 5469−5478.

(15) Zhang, W.; Xiao, X.; Zheng, L.; Wan, C. Fabrication of TiO_2/MoS_2@ Zeolite Photocatalyst and Its Photocatalytic Activity for Degradation of Methyl Orange under Visible Light. *Appl. Surf. Sci.* **2015**, *358*, 468−478.

(16) Qiu, B.; Zhou, Y.; Ma, Y.; Yang, X.; Sheng, W.; Xing, M.; Zhang, J. Facile Synthesis of the Ti3+ Self-Doped TiO_2-Graphene Nanosheet Composites with Enhanced Photocatalysis. *Sci. Rep.* **2015**, *5*, 8591−8596.

(17) Chen, J.; Wen, Y.; Guo, Y.; Wu, B.; Huang, L.; Xue, Y.; Geng, D.; Wang, D.; Yu, G.; Liu, Y. Oxygen-Aided Synthesis of

DOI: 10.1021/acsnano.9b02608
ACS Nano 2019, 13, 6083−6089

Polycrystalline Graphene on Silicon Dioxide Substrates. *J. Am. Chem. Soc.* **2011**, *133*, 17548−17551.
(18) Rümmeli, M. H.; Bachmatiuk, A.; Scott, A.; Börrnert, F.; Warner, J. H.; Hoffman, V.; Lin, J. H.; Cuniberti, G.; Büchner, B. Direct Low-Temperature Nanographene CVD Synthesis over a Dielectric Insulator. *ACS Nano* **2010**, *4*, 4206−4210.
(19) Sun, J.; Gao, T.; Song, X.; Zhao, Y.; Lin, Y.; Wang, H.; Ma, D.; Chen, Y.; Xiang, W.; Wang, J. Direct Growth of High-Quality Graphene on High-κ Dielectric $SrTiO_3$ Substrates. *J. Am. Chem. Soc.* **2014**, *136*, 6574−6577.
(20) Ji, Q.; Zhang, Y.; Gao, T.; Zhang, Y.; Ma, D.; Liu, M.; Chen, Y.; Qiao, X.; Tan, P. H.; Kan, M. Epitaxial Monolayer MoS_2 on Mica with Novel Photoluminescence. *Nano Lett.* **2013**, *13*, 3870−3877.
(21) Lee, Y. H.; Zhang, X. Q.; Zhang, W.; Chang, M. T.; Lin, C. T.; Chang, K. D.; Yu, Y. C.; Wang, J. T. W.; Chang, C. S.; Li, L. J. Synthesis of Large-Area MoS_2 Atomic Layers with Chemical Vapor Deposition. *Adv. Mater.* **2012**, *24*, 2320−2325.
(22) Chen, B.; Yu, Q.; Yang, Q.; Bao, P.; Zhang, W.; Lou, L.; Zhu, W.; Wang, G. Large-Area High Quality MoS_2 Monolayers Grown by Sulfur Vapor Counter Flow Diffusion. *RSC Adv.* **2016**, *6*, 50306−50314.
(23) Fu, Q.; Wang, W.; Yang, L.; Huang, J.; Zhang, J.; Xiang, B. Controllable Synthesis of High Quality Monolayer WS_2 on a SiO_2/Si Substrate by Chemical Vapor Deposition. *RSC Adv.* **2015**, *5*, 15795−15799.
(24) Chen, P.; Xu, W.; Gao, Y.; Warner, J. H.; Castell, M. R. Epitaxial Growth of Monolayer MoS_2 on $SrTiO_3$ Single Crystal Substrates for Applications in Nanoelectronics. *ACS Appl. Nano Mater.* **2018**, *1*, 6976−6988.
(25) Mawlong, L. P. L.; Paul, K. K.; Giri, P. K. Direct Chemical Vapor Deposition Growth of Monolayer MoS_2 on TiO_2 Nanorods and Evidence for Doping-Induced Strong Photoluminescence Enhancement. *J. Phys. Chem. C* **2018**, *122*, 15017−15025.
(26) Yu, Q.; Lian, J.; Siriponglert, S.; Li, H.; Chen, Y. P.; Pei, S.-S. Graphene Segregated on Ni Surfaces and Transferred to Insulators. *Appl. Phys. Lett.* **2008**, *93*, 113103−113105.
(27) Gao, L.; Ren, W.; Xu, H.; Jin, L.; Wang, Z.; Ma, T.; Ma, L.-P.; Zhang, Z.; Fu, Q.; Peng, L.-M.; Bao, X.; Cheng, H.-M. Repeated Growth and Bubbling Transfer of Graphene with Millimetre-Size Single Crystal Grains Using Platinum. *Nat. Commun.* **2012**, *3*, 699−705.
(28) Zhou, X.; Shi, J.; Qi, Y.; Liu, M.; Ma, D.; Zhang, Y.; Ji, Q.; Zhang, Z.; Li, C.; Liu, Z. Periodic Modulation of the Doping Level in Striped MoS_2 Superstructures. *ACS Nano* **2016**, *10*, 3461−3468.
(29) Yu, Y.; Li, C.; Liu, Y.; Su, L.; Zhang, Y.; Cao, L. Controlled Scalable Synthesis of Uniform, High-Quality Monolayer and Few-Layer MoS_2 Films. *Sci. Rep.* **2013**, *3*, 1866−1871.
(30) Ahn, C.; Lee, J.; Kim, H. U.; Bark, H.; Jeon, M.; Ryu, G. H.; Lee, Z.; Yeom, G. Y.; Kim, K.; Jung, J. Low-Temperature Synthesis of Large-Scale Molybdenum Disulfide Thin Films Directly on a Plastic Substrate Using Plasma-Enhanced Chemical Vapor Deposition. *Adv. Mater.* **2015**, *27*, 5223−5229.
(31) Splendiani, A.; Sun, L.; Zhang, Y.; Li, T.; Kim, J.; Chim, C. Y.; Galli, G.; Wang, F. Emerging Photoluminescence in Monolayer MoS_2. *Nano Lett.* **2010**, *10*, 1271−1275.
(32) Mak, K. F.; Lee, C.; Hone, J.; Shan, J.; Heinz, T. F. Atomically Thin MoS_2: a New Direct-Gap Semiconductor. *Phys. Rev. Lett.* **2010**, *105*, 136805.
(33) Kylänpää, I.; Komsa, H. P. Binding Energies of Exciton Complexes in Transition Metal Dichalcogenide Monolayers and Effect of Dielectric Environment. *Phys. Rev. B: Condens. Matter Mater. Phys.* **2015**, *92*, 205418.
(34) Lin, Y.; Ling, X.; Yu, L.; Huang, S.; Hsu, A. L.; Lee, Y.-H.; Kong, J.; Dresselhaus, M. S.; Palacios, T. Dielectric Screening of Excitons and Trions in Single-Layer MoS_2. *Nano Lett.* **2014**, *14*, 5569−5576.
(35) Ochedowski, O.; Marinov, K.; Scheuschner, N.; Poloczek, A.; Bussmann, B. K.; Maultzsch, J.; Schleberger, M. Effect of Contaminations and Surface Preparation on the Work Function of Single Layer MoS_2. *Beilstein J. Nanotechnol.* **2014**, *5*, 291−297.
(36) Borodin, A.; Reichling, M. Characterizing TiO_2 (110) Surface States by Their Work Function. *Phys. Chem. Chem. Phys.* **2011**, *13*, 15442−15447.
(37) Selman, A. M.; Hassan, Z.; Husham, M.; Ahmed, N. M. A High-Sensitivity, Fast-Response, Rapid-Recovery $p-n$ Heterojunction Photodiode Based on Rutile TiO_2 Nanorod Array on p-Si(111). *Appl. Surf. Sci.* **2014**, *305*, 445−452.
(38) Rostami, H.; Moghaddam, A. G.; Asgari, R. Effective Lattice Hamiltonian for Monolayer MoS_2: Tailoring Electronic Structure with Perpendicular Electric and Magnetic Fields. *Phys. Rev. B: Condens. Matter Mater. Phys.* **2013**, *88*, 085440.
(39) Yamamoto, Y.; Nakajima, K.; Ohsawa, T.; Matsumoto, Y.; Koinuma, H. Preparation of Atomically Smooth TiO_2 Single Crystal Surfaces and Their Photochemical Property. *Jpn. J. Appl. Phys.* **2005**, *44*, L511−L514.

DOI: 10.1021/acsnano.9b02608
ACS Nano 2019, 13, 6083−6089